

Stress and Defect Characteristics in Oxide Films and Corrosion Resistance of Zr-1Nb Alloy

Hou Keke¹, Huang Jiao¹, Yao Meiyi^{1,2}, Zhang Junsong³, Sun Rongrong¹,
Zhao Hanpei¹, Long Chongsheng³, Zhang Jinlong^{1,2}, Zhou Bangxin^{1,2}

¹ Institute of Materials, Shanghai University, Shanghai 200072, China; ² Laboratory for Microstructures, Shanghai University, Shanghai 200444, China; ³ Science and Technology on Reactor Fuel and Materials Laboratory, Nuclear Power Institute of China, Chengdu 610213, China

Abstract: Corrosion tests with two approaches of distinct time intervals for heating and cooling in autoclave were carried out to investigate the stress, defect density in the oxide film and corrosion resistance of Zr-1Nb alloy in the 0.01 mol/L LiOH aqueous solution at 360 °C, 18.6 MPa. The stress and defect density in the oxide film were measured by a curl method and the Ion Migration Method (IMM), respectively. Results show that the stress level and defect density in the oxide film in the shorter interval corrosion tests are lower than those in the longer interval corrosion tests at the initial stage of corrosion. The corrosion resistance in the subsequent stages of corrosion is better in the shorter interval corrosion tests. It indicates that at the initial stage of corrosion the mass gain shows no obvious difference between the two approaches of corrosion tests in autoclave under different time intervals for heating and cooling. However, the stress level and defect density in the oxide film exhibit noticeable differences, which leads to two distinct microstructural evolution rates of the oxide film and then results in different corrosion resistance in the subsequent corrosion stages.

Key words: zirconium alloys; corrosion; ion migration method; defects; stress

Zirconium-based alloys have been used for fuel cladding in water-cooled nuclear power plants due to their unique nuclear properties. Their main failure modes during service include waterside corrosion, creep, hydrogen embrittlement, fatigue and so on. The waterside corrosion of zirconium alloy cladding is a main factor affecting the service life of fuel elements^[1].

The oxidation of zirconium occurs at the oxide/metal (O/M) interface. Oxygen ions or hydroxyl ions diffuse through the oxide layer to the O/M interface to react with zirconium to form new zirconium oxide film^[2-4]. Therefore, the characteristics and the microstructural evolution of the oxide film during the corrosion process will affect the corrosion resistance of zirconium alloys. Compressive stress exists inevitably in oxide film due to the Pilling-Bedworth ratio of 1.56 for zirconium. Also, defects such as vacancies

and interstitials form in zirconium oxide crystals. The diffusion, annihilation, and condensation of defects under stress and temperature would occur, which results in the microstructural evolution of oxide film. When vacancies were absorbed by grain boundaries, micro-pore clusters in nano-scale were formed and then further developed into micro-cracks during oxidation. The microstructural evolution causes the relaxation of stress in the oxide film, the acceleration of diffusion of O²⁻ or OH⁻, and the decrease of protective characteristic of the oxide film^[2,4-9]. Thus, it can be seen that the stress and defects affect the microstructural evolution of oxide film and then further influence the corrosion process.

Geng et al.^[10] investigated the effect of corrosion temperature and water chemistry on the compressive stress in oxide film formed on Zircaloy-4 tubular specimens before

Received date: May 25, 2018

Foundation item: National Natural Science Foundation of China (51471102)

Corresponding author: Yao Meiyi, Ph. D., Professor, Institute of Materials, Shanghai University, Shanghai 200072, P. R. China, Tel: 0086-21-56338586, E-mail: yaomeiyi@shu.edu.cn

Copyright © 2019, Northwest Institute for Nonferrous Metal Research. Published by Science Press. All rights reserved.

the thickness was about 2 μm . Results showed that for Zircaloy-4 specimens the compressive stress in the oxide film decreased in the sequence of 360 °C deionized water, 400 °C super-heated steam, and 360 °C lithiated water. It was thought that Li^+ and OH^- ions incorporated into the oxide films decreased the surface free energy of oxide film and higher temperature accelerated the diffusion of defects. As a result, the diffusion of vacancies, formation of pores, and development of micro-cracks were accelerated to make stress relaxation quicker. Hence, corrosion conditions may affect the stress in the oxide film on zirconium alloys and then further influence the growth of oxide film.

Currently, scanning electron microscopy (SEM), transmission electron microscopy (TEM), transmission and back scattering scanning electron microscopy (T-EBSD), electron energy loss spectroscopy (EELS), and three dimensional atom probe (3DAP) are widely used to investigate the growth and evolution process of the oxide layer by observing microstructure of oxide layer, oxidation process of second phase particles and their effect on the microstructure of oxide layer, defects and strain in the oxide layer, the evolution of meta-stable zirconia, and so on^[11-21]. SEM can be used to observe the thickness of oxide film, grain morphology, porosities, and micro cracks. The fine structures of oxide film such as dislocations, grain boundaries, nano-pores, crystal structures and grain orientations can be observed in TEM. However, there are many limitations in the analysis of micro defects in oxide film by SEM and TEM. For example, the observation area is generally limited to less than 10 $\mu\text{m} \times 10 \mu\text{m}$ and the results observed are affected by sample preparation. Most importantly, no quantitative data can be obtained^[22].

Ions have different sizes. If the size of defects in the oxide film is larger than that of ions, the ions will pass through the oxide film. Therefore, the scale and distribution density of defects in the oxide film can be quantitatively analyzed by investigating the migratory behavior of certain ions under the action of electric field, which is denoted as Ion Migration Method (IMM)^[22]. In this research, the internal stress and defect density in the oxide film on zirconium alloys were investigated to further understand the relationship between microstructural evolution of the oxide film and the corrosion resistance of zirconium alloys.

1 Experiment

Zr-1Nb tubular and flaky specimens were corroded by static autoclave tests at 360 °C, 18.6 MPa in 0.01 mol/L LiOH aqueous solution. The specimens were pickled in a mixed acid solution of 10% HF, 30% HNO_3 , 30% H_2SO_4 , and 30% H_2O (volume fraction), and then rinsed in cold tap water. Finally, they were rinsed in boiling deionized water before corrosion tests.

The specimens tested in autoclave were subjected to a

thermal cycle during heating and cooling. The redistribution and relaxation of the stress in the oxide film formed on the specimen can partially occur during thermal cycles. If one specimen was subjected to more thermal cycles than the other in the same period of testing, the stress in the oxide film formed on the specimen subjected to more thermal cycles could be lower. The microstructural evolution of oxide film could be slowed down and the growth of the oxide film would be retarded. Thus, better corrosion resistance for the specimens subjected to more thermal cycles could be expected. The relationship among stress, defects, microstructural evolution in oxide film, and the corrosion resistance will be better understood. Therefore, corrosion tests in autoclave with two approaches of time intervals for heating and cooling were adopted to study the relationship between stress, defects in the oxide film, and the corrosion resistance of zirconium alloys. One approach was to cool down the autoclave by powering it off after a longer time interval, which is defined as longer interval corrosion tests. The other approach was to cool down the autoclave after a relative shorter time interval, which is defined as shorter interval corrosion tests. In a longer interval corrosion test, sample weighing and aqueous solution replacement were conducted at 1st d, 3rd d, 14th d, and then every 30-day interval. The autoclave was cooled down every 30-day periodically. In a shorter interval corrosion test, sample weighing and aqueous solution replacement were carried out at 1st d, 3rd d, 14th d, 44th d, and then every 30-day interval. The autoclave was cooled down from 360 °C to 100 °C at the 2nd d, 6th d, 10th d, and every 10-day interval after a 14 d exposure, and then it was reheated to 360 °C. The operation schedules for autoclave heating and cooling during the longer and shorter interval corrosion tests are shown in Fig.1. Note that the mass gain at 54 d was also measured for the flaky specimens due to their inferior corrosion resistance.

Zr-1Nb tubular specimens were used to study compressive stress in the oxide film by a curl method, while Zr-1Nb flaky specimens were applied to study the defects in the oxide film. When an oxide layer forms on the outer surface of a tubular specimen, the diameter of the tube and its circumference will increase. The compressive stress of oxide is higher in the longitudinal direction than in the circumferential direction because the dimension change of the oxide is less restricted in the circumferential direction than in the longitudinal direction. After the metal matrix is completely removed by immersing the specimens in acid, the oxide layer will curl upwards along the longitudinal direction to form small rolls. By measuring the diameters of the rolls and the thickness of the oxide layers, the stress gradient along the oxide thickness direction can be calculated since the elastic modulus of zirconium oxide is known ($2.06 \times 10^5 \text{ MPa}$ [$30 \times 10^6 \text{ psi}$])^[23,24]. It is assumed that the stress at the outer surface of the oxide film formed on the

tubular specimens is zero and the stress gradient along the thickness remains constant. Therefore, the compressive stress at the O/M interface can be calculated as:

$$\sigma = \mu \frac{t}{r} \tag{1}$$

Where μ is Young's modulus (here $\mu=2.06 \times 10^5$ MPa), t and r represent the thickness and the curvature radius after curling, respectively.

In fact, the above assumption is not strictly true. Only when the oxide film is thick enough, the stress at its outer surface is zero. Moreover, in the process of oxidation, the microstructures of oxide film evolve gradually, which results in the differences in distribution of pores and micro-cracks along the thickness direction of oxide film^[4,7,9]. Therefore, the stress gradient and Young's modulus will vary at different thicknesses of the oxide film. In order to simplify the calculation process, the same Young's modulus is adopted in this study. In fact, there is a difference between the calculated value and the actual value of stress. However, the two values are proportionally correlated, which does not affect the analysis on the change trend of the internal stress of the oxide film in the corrosion process^[10,25].

The fractural surface morphology of the oxidized specimens was examined by a JSM-6700F scanning electron microscope (SEM). The defect density in oxide film was measured by IMM in the Science and Technology on Reactor Fuel and Materials Laboratory in Nuclear Power Institute of China^[22,26]. As shown in Fig.2a, there are positive and negative ions in CuSO₄ aqueous solution. Under the action of the electric field, the positive and negative ions move toward their opposite electrodes to produce a loop current. As the zirconium oxide film contains fewer defects, fewer ions can move through the oxide film, and thus, the impedance is high. On the contrary, when there are more defects in the oxide film, the impedance is low.

The equivalent circuit is shown in Fig.2b. The total current I in the ammeter can be approximated as:

$$I = \frac{VR_v(R_i + R_e)}{R_s(R_iR_v + R_vR_e + R_eR_i) + R_iR_vR_e} \tag{2}$$

Where V is voltage value, R_s is internal resistance of external DC power supply, R_v is internal resistance of the voltmeter, R_e is electron conduction resistance of the oxide film, and R_i is ion migration resistance in the oxide film.

The total current I mainly consists of electron conduction current I_e and ion migration current I_i . If the oxide film does not have macro-defects, the electron conduction resistance of the oxide film is very large (more than $3 \times 10^9 \Omega$) and I_e is very small. For the zirconium oxide film with about 2 μm in thickness, the I_e is less than 500 nA at 40 V and the I_e is less than 50 nA under the 10 V voltage by the hollow electrode with inner cavity radius of 6 mm when filled with liquid

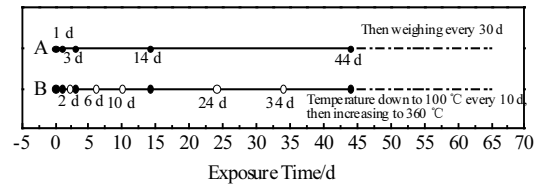


Fig.1 Schematic diagram showing longer (A) and shorter (B) interval corrosion tests in autoclave for heating and cooling at 360 °C, 18.6 MPa in 0.01 mol/L LiOH aqueous solution (solid dot on behalf of weighing time, open dot on behalf of operation time with cooling and reheating)

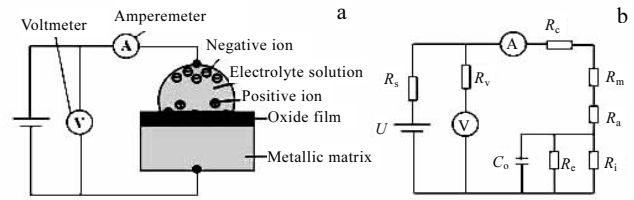


Fig.2 Principle of Ion Migration Method (a) and the equivalent circuit diagram (b)^[22,26]

Note: R_c is internal resistance of the ammeter, R_m is equivalent resistance of the metal substrate circuit, R_a is equivalent resistance of the electrolyte solution

metal gallium (Ga). Therefore, the total current I mainly depends on I_i and the micro-defects in the oxide film have great impact on I_i ^[22,26].

2 Results and Discussion

2.1 Corrosion behavior of Zr-1Nb alloy

Fig.3 shows the corrosion mass gain curves of Zr-1Nb alloy specimens in 0.01 mol/L LiOH aqueous solution at 360 °C, 18.6 MPa. The mass gain of Zr-1Nb tubular specimens is about 62.6 mg/dm² for 164 d exposure in the shorter interval corrosion tests, which is 82.7% less than that (360.1 mg/dm²) in the longer interval corrosion tests. For the flaky specimens, the mass gain in the shorter interval corrosion tests is 803.8 mg/dm² for 74 d exposure, which is 22.3% less than that (1034.8 mg/dm²) in the longer interval corrosion tests. The corrosion resistance of tubular specimens is better than that of flaky specimens under two approaches of autoclave tests. For both tubular and flaky specimens, their corrosion resistance in the shorter interval corrosion tests is obviously better than that in the longer interval corrosion tests. The difference in corrosion resistance may be correlated to the stress state in the oxide film of flaky and tubular specimens in the two testing approaches.

2.2 Cross-sectional microstructure of oxide film

Fig.4 shows the cross-sectional micro-structure of the oxide film formed on Zr-1Nb tubular specimens in the short

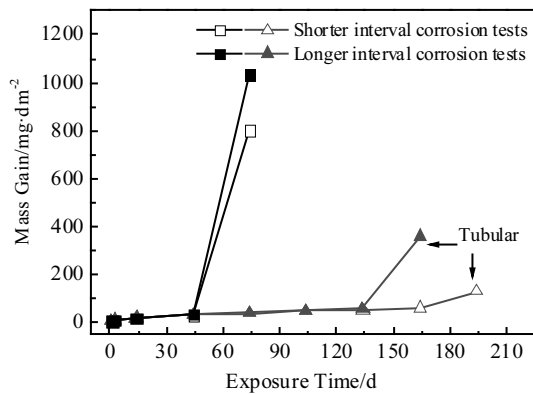


Fig.3 Mass gain vs exposure time of Zr-1Nb alloy specimens in two approaches of autoclave tests in lithiated water with 0.01 mol/L LiOH at 360 °C and 18.6 MPa

interval corrosion tests for 74 d exposure. The average thickness of oxide film is 2.68 and 2.75 μm at the outer and inner wall of Zr-1Nb tube, respectively, which indicates that there is little difference between them. Micro-cracks are observed in certain local areas and the cross section of the oxide film is relatively flat.

Fig.5 shows the cross-sectional micro-structure of the oxide film formed on Zr-1Nb tubular specimens in the longer interval corrosion tests. The average thickness of the oxide film at the outer and inner wall is 2.82 and 2.79 μm, respectively, which shows little difference. The oxide layer mainly consists of columnar grains and the number of equiaxed grains is small. Compared with Fig.4, more cracks and pores appear on the oxide fractural surface with obvious undulations, which is indicated by the arrows in Fig.5b, 5d. The corrosion rate will be accelerated when O²⁻ or OH⁻ invade into the O/M interface through these micro-cracks and pores.

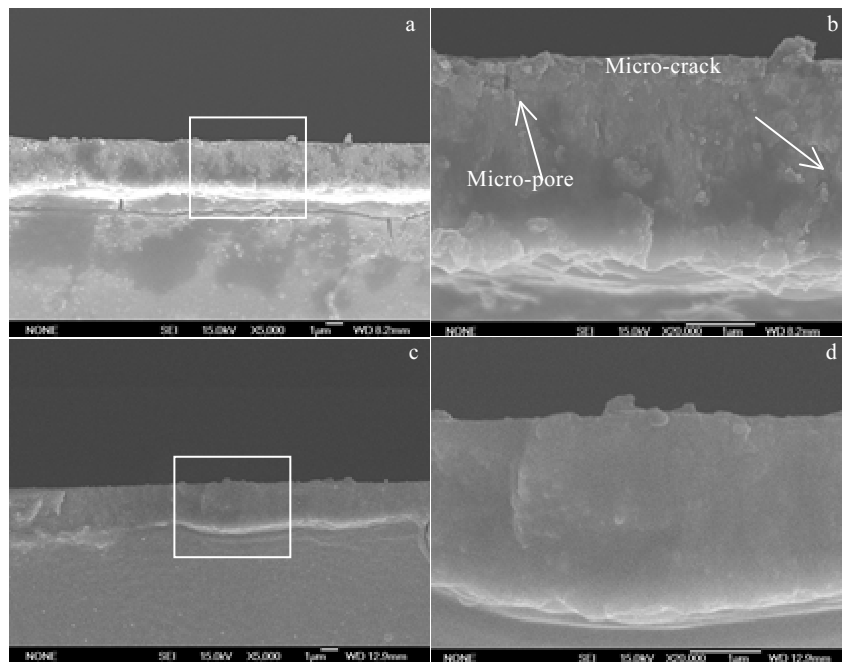


Fig.4 Fractal morphologies of the oxide films on the outer (a, b) and inner (c, d) walls on Zr-1Nb tubular specimen corroded for 74 d in lithiated water with 0.01 mol/L LiOH at 360 °C and 18.6 MPa under shorter interval corrosion tests

2.3 Internal stress and defects in the oxide film on Zr-1Nb alloy specimens

Fig.6 exhibits internal stress v s thickness of oxide film on Zr-1Nb tubular specimens in the two approaches of corrosion tests. It is clear that the internal stress in the oxide film decreases gradually when the thickness of oxide film increases. It can also be seen that the thickness of the oxide film for specimens corroded by two different approaches shows little difference before 44 d exposure. However, the stress level in the shorter interval corrosion

tests is always lower than that in the longer interval corrosion tests. Besides, quicker stress relaxation occurs in the shorter interval corrosion tests. These results illustrate that increasing the frequency of the thermal cycles can indeed accelerate the relaxation of internal stress in the oxide film to reach a lower stress level. Moreover, while the mass gain has no difference between two approaches of corrosion tests before an exposure of 44 d (see Fig.3), the stress level in the oxide film has exhibited some differences.

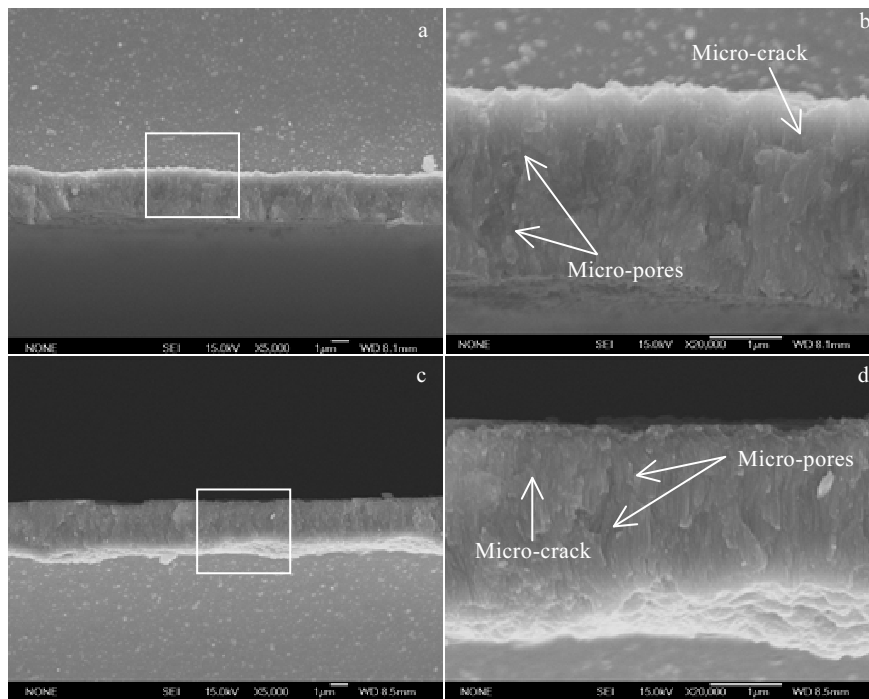


Fig.5 Fractal morphologies of the oxide films on the outer (a, b) and inner (c, d) walls on Zr-1Nb tubular specimen corroded for 74 d in lithiated water with 0.01 mol/L LiOH at 360 °C and 18.6 MPa under longer interval corrosion tests

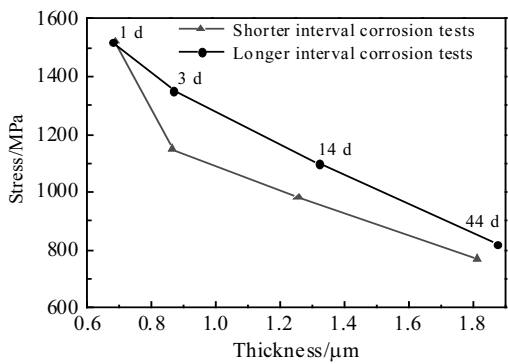


Fig.6 Internal stress in the oxide films of Zr-1Nb tubular specimens corroded by two ways of autoclave tests in lithiated water with 0.01 mol/L LiOH at 360 °C and 18.6 MPa

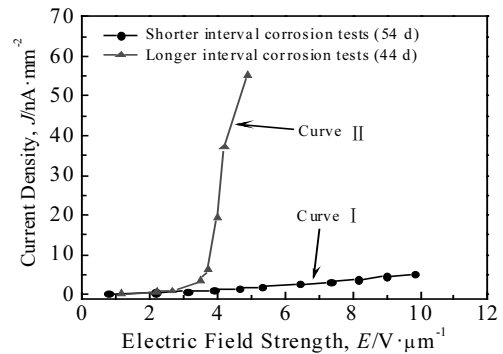


Fig.7 *J-E* curves of the oxide film on Zr-1Nb flake specimens under two ways of autoclave tests in lithiated water with 0.01 mol/L LiOH at 360 °C and 18.6 MPa

The flaky specimens for 44 d exposure in the longer interval corrosion tests and 54 d exposure in the shorter interval corrosion tests were selected to study the defects in the oxide film. The mass gain of the former is 34.37 mg/dm², while the mass gain of the latter is 54.11 mg/dm² as shown in Fig.3. Current density (*J*)-electric field intensity (*E*) curves of the oxide film on Zr-1Nb flaky specimens in the two approaches of corrosion testing are shown in Fig.7. The onset of current breakaway of the curve directly reflects the micro-defect density in the oxide film. A small *E* value of onset

of the curve reflects a higher defect density in the oxide film. The *E* value of onset for curve II is about 4 V/µm, while that for curve I is above 10 V/µm. It means that the defect density in the oxide film after corrosion for 54 d exposure in the shorter interval corrosion tests is obviously lower than that for 44 d exposure in the longer interval corrosion tests. However, the mass gain of the former is a little higher than that of the latter.

At the initial stage of corrosion, although the mass gains in two approaches of autoclave tests have little difference

(Fig.3), the stress and micro-defects in the oxide film are significantly different (Fig.6 and 7). These differences lead to different microstructural evolution rates of oxide films at the later stage of corrosion. In the shorter interval corrosion tests, the compressive stress level in the oxide film is lower at the initial stage of corrosion (Fig.6), which results in fewer defects in the oxide film (Fig.7). Meanwhile, the lower compressive stress slows down the formation of micro-pores and micro-cracks by delaying the diffusion, annihilation and condensation of defects in the oxide film. In the longer interval corrosion tests, the compressive stress level in the oxide film is higher, which not only results in more defects in the oxide film but also accelerates the formation of micro-pores and micro-cracks in the oxide film. SEM observation on the fractural surface of oxide film shows that more micro-pores and micro-cracks appear on the fracture surface of oxide film formed on the specimens in the longer interval corrosion tests (Fig.5).

Accordingly, the corrosion rate of the specimens at the later exposure time is faster in the longer interval corrosion tests (Fig.3). This further illustrates that the stress level and defect density in the oxide film are important factors in affecting the corrosion resistance of zirconium alloys, and the relationship between the corrosion resistance and the stress as well as defect density in the oxide film formed on zirconium alloys can be studied by different approaches of autoclave tests with distinct time intervals for heating and cooling.

Moreover, it has been reported that Zr-Nb series alloys exhibit very poor corrosion resistance in lithiated water with 0.01 mol/L LiOH at 360 °C, 18.6 MPa. The corrosion rate of the alloy increased significantly after corrosion transition, and the mass gain reached hundreds of milligrams per square decimeter for dozens of day exposure^[27-29]. The reason has been explained in our previous work from the viewpoint of the oxidation of β -Nb particles and the dissolution of oxidation production Nb_2O_5 ^[13,29-33].

3 Conclusions

1) The relationship between the stress, defect density in the oxide film and the corrosion resistance of the Zr-1Nb alloy specimens was studied by different approaches of autoclave tests with distinct time intervals for heating and cooling. When Zr-1Nb alloy is corroded in 0.01 mol/L LiOH aqueous solution at 360 °C, 18.6 MPa, at the initial stage of corrosion there are differences in the stress level and defect density in the oxide film in different approaches of autoclave tests. In the shorter interval corrosion tests, the stress level and defect density in the oxide film are both lower than that in the longer interval corrosion tests, which lead to better corrosion resistance in the later corrosion stage.

2) The mass gains from the two testing approaches are

similar in the initial stage of corrosion. However, the stress and defects in the oxide film have obvious differences, which lead to different microstructural evolution rates of the oxide film. Consequently, corrosion resistance of the alloy differs at the later corrosion stage.

References

- 1 IAEA-TECDOC-996. *Waterside Corrosion of Zirconium Alloys in Nuclear Power Plants*[R]. Vienna: International Atomic Energy Agency, 1998: 1011
- 2 Zhou Bangxin, Li Qiang, Liu Wenqing et al. *Rare Metal Materials and Engineering*[J], 2006, 35(7): 1009 (in Chinese)
- 3 Ni N, Lozano-Perez S, Jenkins M L et al. *Scripta Materialia*[J], 2010, 62: 564
- 4 Zhou B X, Li Q, Yao M Y et al. *15th International Symposium*[C]. West Conshohocken: ASTM STP 1505, 2008: 360
- 5 Du Chenxi, Peng Jianchao, Li Hui et al. *Acta Metallurgica Sinica*[J], 2011, 47(7): 887 (in Chinese)
- 6 Zhou Bangxin, Li Qiang, Yao Meiyi et al. *Corrosion and Protection*[J], 2009, 30(9): 589 (in Chinese)
- 7 Zhou B X, Li Q, Huang Q et al. *Nuclear Power Engineering*[J], 2000, 21(5): 439 (in Chinese)
- 8 Zhou B X, Peng J C, Yao M Y et al. *16th International Symposium*[C]. West Conshohocken: ASTM STP 1529, 2011: 620
- 9 Zhou B X, Li Q, Yao M Y et al. *Nuclear Power Engineering*[J], 2005, 26(4): 364 (in Chinese)
- 10 Geng J Q, Zhou B X, Yao M Y et al. *Journal of Shanghai University*[J], 2011, 17(3): 291 (in Chinese)
- 11 Gou S Q, Zhou B X, Chen C M et al. *Corrosion Science*[J], 2015, 92(3): 237
- 12 Hu J, Garner A, Ni A N et al. *Micron*[J], 2015, 69(12): 35
- 13 Sun G C, Zhou B X, Yao M Y et al. *Acta Metallurgica Sinica*[J], 2012, 48(9): 1103 (in Chinese)
- 14 Dong Y, Motta A T, Marquis E A. *Journal of Nuclear Materials*[J], 2013, 442(11): 270
- 15 Kim H G, Choi B K, Park J Y et al. *Journal of Alloys & Compounds*[J], 2009, 481(7): 867
- 16 Yardley S S, Moore K L, Ni N et al. *Journal of Nuclear Materials*[J], 2013, 443(11): 436
- 17 Vermaak N, Parry G, Estevez R et al. *Acta Materialia*[J], 2013, 61(7): 4374
- 18 Polatidis E, Frankel P, Wei J et al. *Journal of Nuclear Materials*[J], 2013, 432(1): 102
- 19 Chen L Y, Li J X, Zhang Y et al. *Corrosion Science*[J], 2015, 100(11): 651
- 20 Annand K J, MacLaren I, Gass M. *Journal of Nuclear Materials*[J], 2015, 465(10): 390
- 21 Nicholls R J, Ni N, Lozano-Perez S et al. *Advanced Engineering Materials*[J], 2015, 17(2): 211
- 22 Long C S, Wei T G, Chen H S et al. *Nuclear Power*

- Engineering[J], 2016, 37(2): 87 (in Chinese)
- 23 Zhou B X. *Journal of Chinese Society of Corrosion and Protection*[J], 1990, 10(3): 197
- 24 Bradhurst D H, Heuer P M. *Journal of Nuclear Materials*[J], 1970, 37(10): 35
- 25 Liu W Q, Li Q, Zhou B X et al. *Rare Metal Materials and Engineering*[J], 2004, 33(10): 1112 (in Chinese)
- 26 Long C S, Wei T G, Chen H S. *Method and Apparatus for Quantitatively Measuring Micro Defect of Oxide Film. China Patent, 201510376679.9*[P], 2015 (in Chinese)
- 27 Bojinov M, Karastoyanov V, Kinnunen P et al. *Corrosion Science*[J], 2010, 52(1): 54
- 28 Sun F T, Yao M Y, Long X et al. *Journal of Shanghai University*[J], 2015, 21(2): 182 (in Chinese)
- 29 Yao M Y, Gao C Y, Huang J et al. *Corrosion Science*[J], 2015, 100(11): 169
- 30 Huang J, Yao M Y, Gao C Y et al. *Corrosion Science*[J], 2016, 104(3): 269
- 31 Caldwell L C, Caldwell P. *Journal of Nuclear Materials*[J], 2013, 432(1): 222
- 32 Huang J, Yao M Y, Gao C Y et al. *Corrosion Science*[J], 2015, 99(10): 172
- 33 Yu J, Liu X Q. *Materials Letters*[J], 2007, 61(1): 355

Zr-1Nb 合金的耐腐蚀性能与氧化膜中应力和缺陷的关系

侯可可¹, 黄 娇¹, 姚美意^{1,2}, 张君松³, 孙蓉蓉¹, 赵寒沛¹, 龙冲生³, 张金龙^{1,2}, 周邦新^{1,2}

(1. 上海大学 材料研究所, 上海 200072)

(2. 上海大学 微结构重点实验室, 上海 200444)

(3. 中国核动力研究设计院反应堆燃料与材料重点实验室, 四川 成都 610213)

摘 要: 采用2种时间间隔加热和冷却高压釜的腐蚀试验研究了Zr-1Nb合金在360 °C, 18.6 MPa, 0.01 mol/L LiOH水溶液中的耐腐蚀性能; 用卷曲法测量了氧化膜中的应力; 利用离子迁移方法 (IMM) 测量了氧化膜中的缺陷数量。结果表明: 在腐蚀初期, 短时间间隔方式下样品氧化膜中的应力水平和缺陷密度都比长时间间隔方式下的低, 前者在腐蚀后期表现出更佳的耐腐蚀性能。这说明在2种时间间隔方式下, 腐蚀初期样品的增重在没有明显差别的情况下, 氧化膜中的应力水平和缺陷密度均已存在显著的差别, 从而造成氧化膜显微组织演化速率的不同, 进而引起合金耐腐蚀性能的差别。

关键字: 锆合金; 腐蚀; 离子迁移方法; 缺陷; 应力

作者简介: 侯可可, 男, 1990年生, 硕士, 上海大学材料研究所, 上海 200072, 电话: 021-56338586, E-mail: hkk0510@163.com